AIMS Materials Science, 6(6): 1033–1048.
DOI: 10.3934/matersci.2019.6.1033
Received: 01 September 2019
Accepted: 21 October 2019
Published: 30 October 2019

http://www.aimspress.com/journal/Materials

Research article

Influence of infill density on microstructure and flexural behavior of 3D printed PLA thermoplastic parts processed by fusion deposition modeling

Bandar Abdullah Aloyaydi[1,*], Subbarayan Sivasankaran[1,*] and Hany Rizk Ammar[1,2]

[1] Digital Manufacturing Laboratory，Mechanical Engineering Department, Qassim University, Buraidah 51452, Saudi Arabia
[2] Metallurgical and Materials Engineering Department, Faculty of Petroleum and Mining Engineering, Suez University, Suez, Egypt

* **Correspondence:** Email: aloyaydi@qu.edu.sa; sivasankarangs1979@gmail.com;
Tel: +966502180020; +966534810975.

Abstract: The main goal of the present work was to investigate the influence of infill density (ID) on microstructure and flexural behavior of 3D printed parts by conducting three points bending test (3PBT). Flexural behavior of 3D printed parts is mainly dependent on ID which applied during printing. A thermoplastic of poly-lactic acid (PLA) was selected as material which can be best suitable for artificial tissue/bone engineering applications. Further, most of the artificial bones/tissues are subjected to fail due to bending load. Therefore, the effect of ID on the flexural strength of PLA (Bio-degradable) materials is important; which was addressed through this research work. Here, the PLA material was printed using fusion deposition modeling (FDM) by varying ID (40, 60, 80, and 100%). The 3D printed cylindrical specimen of 15 mm in diameter and 30 mm span was used. The bending responses in terms of bending stress-strain and bending force-deflection at each ID were investigated and reported. Furthermore, the fracture bending stress, fracture bending strain, flexural modulus, and stiffness of the printed sample were measured and correlated to the ID. The experimental result has shown that the bending characteristics influenced a strong correlation with ID percentage. The result suggested that the 80% ID was the optimum percentage which possessed considerable strength and toughness. Besides, the specimen surface morphology and the fracture topography were investigated and reported.

Keywords: poly-lactic acid; fusion deposition modeling, infill density; bending stress-strain; microstructure

Abbreviations: AMT: Additive manufacturing technology; FDM: Fusion deposition modeling; ID: Infill density; ABS: Acrylonitrile butadiene styrene; PLA: poly-lactic acid; PA: Polyamide; PEEK: Polyether ether ketone; PETG: Polyethylene terephthalate glycol; HIPS: High impact polystyrene resin; 3PBT: 3-points bending test; FEG-SEM: Field emission gun scanning electron microscope; FTM: Film thickness monitor

1. Introduction

The demand for using additive manufacturing technology (AMT) has increased steeply in recent years compared to the last decade [1]. In AMT, the products are made layer-by-layer by which all kinds of intricate parts can be easily manufactured which cannot be fabricated by conventional subtractive processes [2]. AMT has several techniques to build the products in which the common technique is fusion deposition modeling (FDM) [3]. The FDM was invented in 1992 by American Company Stratays [4]. The process of building an object in FDM is to heat a strip of thermoplastic material and then extruded the melting material via a nozzle to build the object layer-by-layer in the build platform under a robust machine control system. The nozzle and build platform moves continuously and simultaneously in x, y, and z-direction to build the desired object [5]. Nowadays, the FDM process is being used to fabricate the parts in aerospace, automotive, spacecraft, and bioengineering industries [6]. Because of these applications, examining the mechanical property of 3D printed parts to check the capability under mechanical loading is necessary [7]. The FDM process possesses the major features of scalability and material flexibility. However, the part quality and anisotropic characteristics in nature are the main challenges in FDM. Several parameters are influencing the mechanical performance of 3D printed parts which are build orientation (flat, edge and upright), extrusion temperature, layer thickness, nozzle diameter, printing velocity, infill density (ID), type of infill pattern, environmental conditions, raster/ infill orientation (0, 45 and 90o), top and bottom cover thickness [8–10]. Based on the literature, it was found that the build orientation should ensure the large contact area of a specimen with the platform while printing by which improved mechanical properties can be obtained [11]. The flat and edge build orientation can ensure a large contact area in which the flat build orientation can print the parts without any manufacturing difficulties as compared to the edge build orientation [12]. Tymrak et al. [13] investigated the mechanical behavior of acrylonitrile butadiene styrene (ABS) and poly-lactic acid (PLA) plastics by varying layer thickness and build orientation. The results were explained that the tensile strength was decreased with the function of layer thickness and improved mechanical strength was obtained at 0.20 mm layer thickness with flat build orientation. Lanzotti et al. [3] examined the tensile strength of PLA 3D printed parts by FDM in which build orientation and layer thickness were varied. The observed results explained that the maximum ultimate tensile strength of around 51MPa was obtained when the layer thickness was 0.15mm and infill/raster orientation was 45 °. Sood et al. [11] studied the mechanical behavior of ABS 3D printed plastic parts by FDM in terms of tensile test, impact test, and flexural test. The results were concluded that the tensile strength was increased when decreasing layer thickness whereas the flexural strength and impact strength were increased with

increasing layer thickness. Fernandez Vicente et al. [14] examined the influence of infill pattern on the mechanical behavior of ABS 3D printed plastics by FDM by conducting a tensile test. The various infill patterns such as line, rectilinear, and honeycomb were taken for investigation. The results were revealed that the line and honeycomb infill pattern samples were produced improved mechanical properties when compared to rectilinear. Ahn et al. [2] studied the anisotropic mechanical behavior of ABS 3D printed plastics by FDM in terms of tensile and compressive strength. The authors varied the raster/infill orientation, air gap, color of the material, bead width, and extruded temperature. The results were concluded that the raster orientation and air gap were the most influencing parameters on mechanical strength when compared to other variables. Ziemian et al. [15] investigated the raster/infill orientation on the mechanical properties of ABS 3D printed plastics by FDM. The mechanical properties (tensile, compressive, flexural, impact, and fatigue strengths) were examined and reported the optimal raster angle for having improved mechanical properties. Tsouknidas et al. [16] studied the impact absorption of PLA samples printed by the FDM machine with different printing speeds. The PLA samples were subjected to the compression load. The study has shown that the lowest printing speed given the highest tensile strength. Torres et al. [17] evaluate the effect of the layer thickness, ID, and heat treatment of the PLA specimen printed by FDM on the mechanical properties (stress-strain) examined by the torsion test. The experiment was conducted using the Taguchi method to control the various process parameters. In addition, the applications of artificial intelligence techniques and various optimization methods are being applied to monitor/control the FDM process during printing [18]. The materials used for 3D printed parts also influence the mechanical behavior in addition to various process parameters. Thermoplastics are the commonly used materials for 3D printing by the FDM process. Among the several thermoplastics, namely, ABS, PLA, polyamide (PA, nylon), polyether ether ketone (PEEK), polyethylene terephthalate glycol (PETG), and high impact polystyrene resin (HIPS), PLA is a commonly used material for studying purpose. Further, PLA is a biodegradable one that can be best suitable for tissue/bone engineering applications [19,20]. Based on the literature, though some authors have investigated the mechanical behavior of ABS and PLA, there is no work related to varying ID on the flexural behavior of PLA 3D printed parts by FDM. Therefore, the present research work investigates the mechanical behavior of the PLA 3D printed parts using the 3-points bending test (3PBT). The ID of 40%, 60%, 80%, and 100% were varied. The cylindrical PLA specimen was printed with a base of 15 mm and a height of 40 mm.

2. Materials and method

2.1. Design, FDM printer, and material

The specimen for 3PBT was designed with a dimension of 15 mm in diameter and 40 mm in height using the Solidwork® software. After that, the designed specimen was imported in the Cura® software to select the desired slicing printing parameters. The parameters used during printing the specimen in the present study are illustrated in Table 1. The ID was varied from 40% to 100% with a step of 20%. The cylindrical sample was printed vertically with a height of 40 mm as more contact area was obtained in this orientation. At least, three repeated samples in each ID were used and the average was used for investigation. The machine used in this study was Desktop Witbox2 Ultimaker, supplied by BQ from Spain. The maximum printing volume of the machine is 297 × 210 × 200 mm.

The machine build platform is an un-heat able one. Hence, to improve the adhesion between the bottom layers of the printed sample and the machine platform, a paper of adhesive tape was used and replaced after each printing. The general schematic diagram of the FDM printing is explained in Figure 1.

Table 1. The fixed parameters used in Fusion Deposition Modeling of 3D printer.

Variable	Selected	Variable	Selected
Material type	PLA	Infill pattern	Line
Filament diameter	1.75 mm	Layer height	200 μm
Platform adhesion type	Brim	Extruder temperature	200 ℃
Nozzle diameter	0.4 mm	Printing speed	20 mm/s
Platform temperature	RT, @22 ℃	Air flow cooling	100 %
Build orientation	Flat	Heated bed temperature	N/A
Raster angle	0 °		

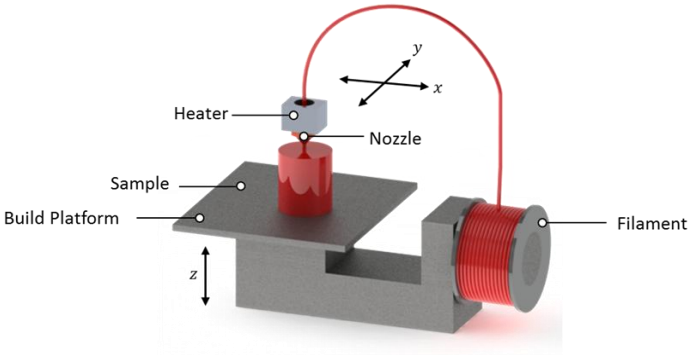

Figure 1. A general schematic diagram of the FDM process.

A thermoplastic PLA filament with a diameter of 1.75 mm was used to build the specimens. The PLA spool was exposed to the air during printing the specimen. The physical and mechanical properties of the raw PLA filament are stated in Table 2 which was as received from the BQ supplier.

Table 2. Physical and mechanical properties of PLA filament as stated from the supplier.

Properties	Values
Density	1.24 g/cm^3
Tensile strength	60 MPa
Flexural Strength	108 MPa
Elongation	9%
Young's modulus	3100 MPa
Shore hardness	85 Sh D
Melting temperature	145–160 ℃
Glass transition temperature	56–64 ℃

2.2. Three points bending test

The 3PBT experiment was conducted using the MTS machine of model number 370.25 which

was supplied by MTS Systems Corporation. The capacity of the actuator force is 250 KN. The dynamometer was embedded on the upper (moving) platen to measure the applied vertical force. To conduct a flexural test for a tiny sample, a fixture was designed and fabricated. The schematic of 3PBT is shown in Figure 2 and the test was conducted as per the ASTM D790 standard [21]. The 3PBT fixture has consisted of two main parts: one part is called a loading pin and the second part is called supporting pins. These two parts were attached to the MTS machine as shown in Figure 2. The loading pin was attached to the moving top platen and the supporting fixture was attached to the bottom platen. The thickness of the loading pin and supporting pins are 5 mm with hemispherical ends. Before executing the experiment, the specimen lied horizontally on the fixture support with span length (distance between the pins support) of 30 mm. The applied load performed at the center of the span length with a speed of 1 mm/min (i.e. 1.11×10^{-3} s^{-1}) [22]. All experiments were executed at 25 ℃. The specimen and 3PBT fixture parameters are illustrated in Table 3. The induced bending stress was calculated using the Eq 1:

$$\sigma_b = \frac{8WL}{\pi d^3} \tag{1}$$

where W is the applied bending load at the center of the specimen in N, L is the distance between the support (span) in mm, d is the diameter of the specimen in mm. Further, the induced bending strain was determined using Eq 2:

$$\varepsilon_b = \frac{6\delta d}{L^2} \tag{2}$$

where δ is the measured deflection at the mid-span of the specimen in mm. Besides, the flexural modulus (E_b) was calculated using Eq 3:

$$E_b = \frac{4L^3 m}{3\pi d^4} \tag{3}$$

where m is the first linear slope from the bending load-deflection curve which was determined between 0.25 W_{max} and 0.75 W_{max} [12].

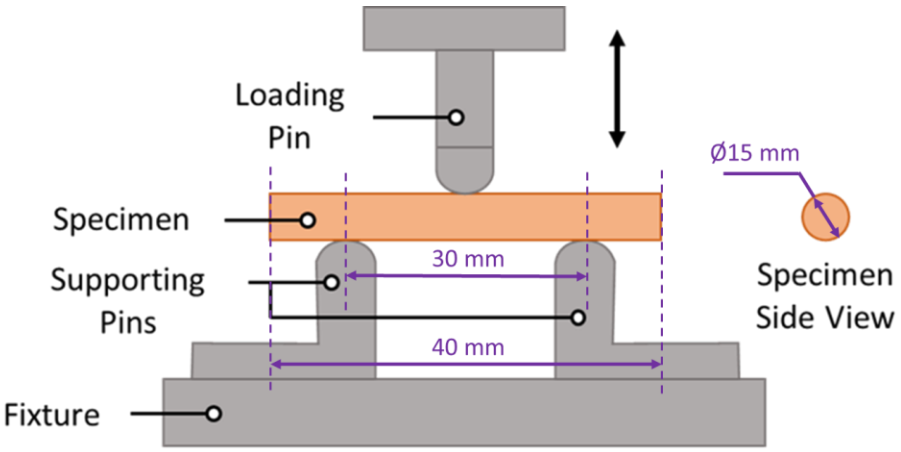

Figure 2. Schematic diagram of 3PBT fixture.

Table 3. Specimen and 3PBT fixture dimension.

Parameters	Value
Loading pin diameters	5 mm
Supporting pin diameters	5 mm
Span length	30 mm
Temperature environment	25 ℃
Specimen dimension diameter	15 mm

2.3. Microstructure

The topography of as-printed PLA samples for checking the printing quality characteristics as per designed input and the fractured surface morphology were observed using Apreo LoVac-field emission gun scanning electron microscope (FEG-SEM, 30 keV, resolution of 1.3 nm at 1 kV). As PLA is plastic and to avoid charging during the capturing of images in FEG-SEM, before loading the samples, the samples were coated with a 15 nm gold film using a film thickness monitor (FTM, sputtering). The sputtering machine used was the Q150T Turbo-pumped sputter coating device.

3. Results and discussion

3.1. Surface topography investigation

Figure 3 shows the surface topography of as-printed PLA parts at different ID (40%, 60%, 80%, and 100%). From Figure 3, the set line type infill pattern was seen from the deposited bead. From Figure 3, the plan view of surface topography was clearly shown that the build orientation among the layers was 90 ° (vertical one). Besides, no surface defects such as cracks, voids or damages were observed over the printed layers which ensured the good quality characteristics of the FDM printer used in the current study. The observed air gap was started to decrease with the function of the ID. Moreover, effective bonding between the two layers was also achieved (Figure 3). The geometry of printed layer thickness and layer height was also measured and correlated with the nozzle diameter [2]. The set layer height was 0.2 mm whereas the nozzle diameter was 0.4 mm and hence, the printed layer cross-section was in elliptical. Top surface topography of 40% ID sample (Figure 3a) was produced non-uniform deposited bead width due to the presence of more air gap between two layers. This air gap in the 40% ID sample was related to the extruded material from the nozzle flowed freely and occupied more space during deposition. However, the observed air gap was disappeared with the function of the ID. Almost, 100% ID sample (Figure 3d) produced uniform deposition of bead width due to no air gap during the deposition of material from the nozzle. In a 100% ID sample, the extruded material from the nozzle cannot flow freely over the layer due to restriction of flow by the adjacent layers and hence, effective bonding among all the layers was achieved without air gap.

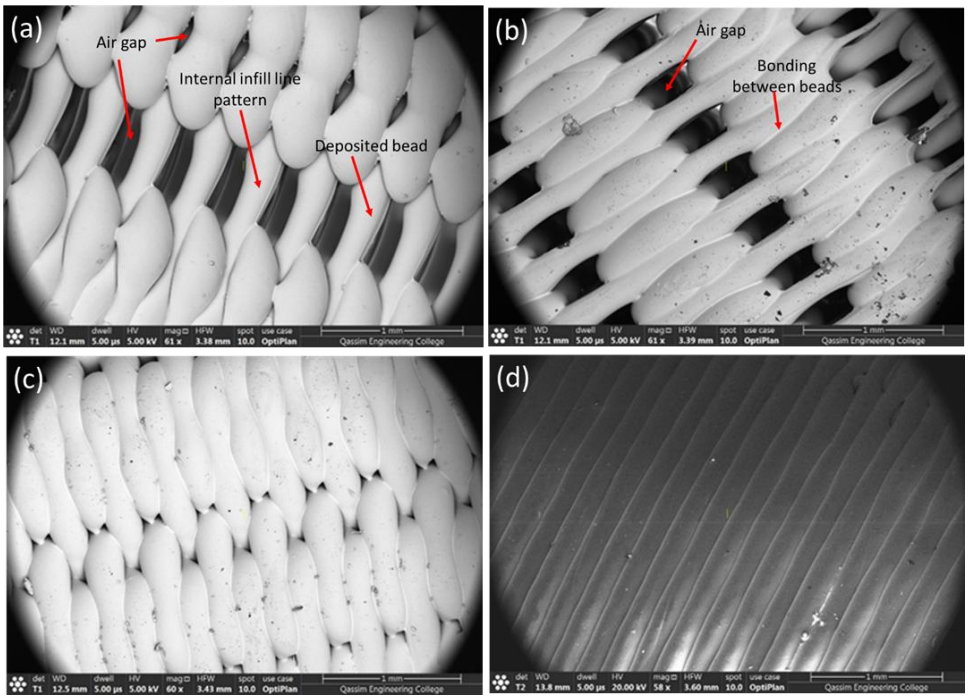

Figure 3. The surface topography of as-printed cylindrical PLA samples with different infill density of: (a) 40%, (b) 60%, (c) 80%, and (d) 100%.

3.2. Flexural behavior

The product quality mainly depends on several factors in which 3D printing machine process parameters influence more on the mechanical behavior of PLA parts [23]. The objective of this research was to study the effect of the ID percentage on flexural behavior by conducting 3PBT. The desired ID percentage was 40%, 60%, 80%, and 100%. Fixing the volume of the PLA specimen, increasing the ID percentage (decreasing the porosity) leads to an increase in the amount of material which creates more node contact (two-layer cross each other) and more layer in the fixed volume (see Figure 3). The flexural bending stress-strain responses of the 3PBT at different ID percentages are shown in Figure 4 which was determined using Eqs 1 and 2. The flexural bending stress-strain curves (Figure 4) clearly shown that the characteristic response of the bending stress-strain with the function of ID. The characteristics response values of the 3PBT are also stated in Table 4. As it can be seen in Figure 4, the slope of the bending stress-strain responses increased gradually as the ID percentage increased. Three replicas in each ID percentage were used in this research and the average was used for investigation. It was ensured during the 3PBT that all the PLA specimens were broken completely at the mid of the span. The observed results were explained that the peak bending stress was increased as the ID increased. For example, the peak bending stress for 40% and 100% was 8.90 MPa and 90.54 MPa, respectively. The resistance to the bending fracture stress in a 100% ID sample increased approximately 10 times compared to the 40% ID sample. This result confirms that the ID percentage was influenced significantly on bending fracture stress. Further, there was not much variation in the peak bending stress between 40% and 60% ID samples (Table 4). However, 80% and 100% ID samples produced more peak bending stress. This result was due to the presence of more layers, decreased porosity percentage, and more bonding

strength among the layers when compared to 40% and 60% ID samples. Similarly, observed peak bending strain-to-failure was increased slightly with the function of ID except for the 60% ID sample. This was due to the domination of bonding strength among the layers. However, the 60% ID sample was produced bending strain-to-failure of 17.32 mm/mm which was the lowest one among other samples. This was due to less deflection during load at the center. However, the 40% ID sample was produced more bending strain-to-failure when compared to the 60% ID sample. This was due to the domination of more porosity in the sample in which the presence of more porosity increases the deflection before failure.

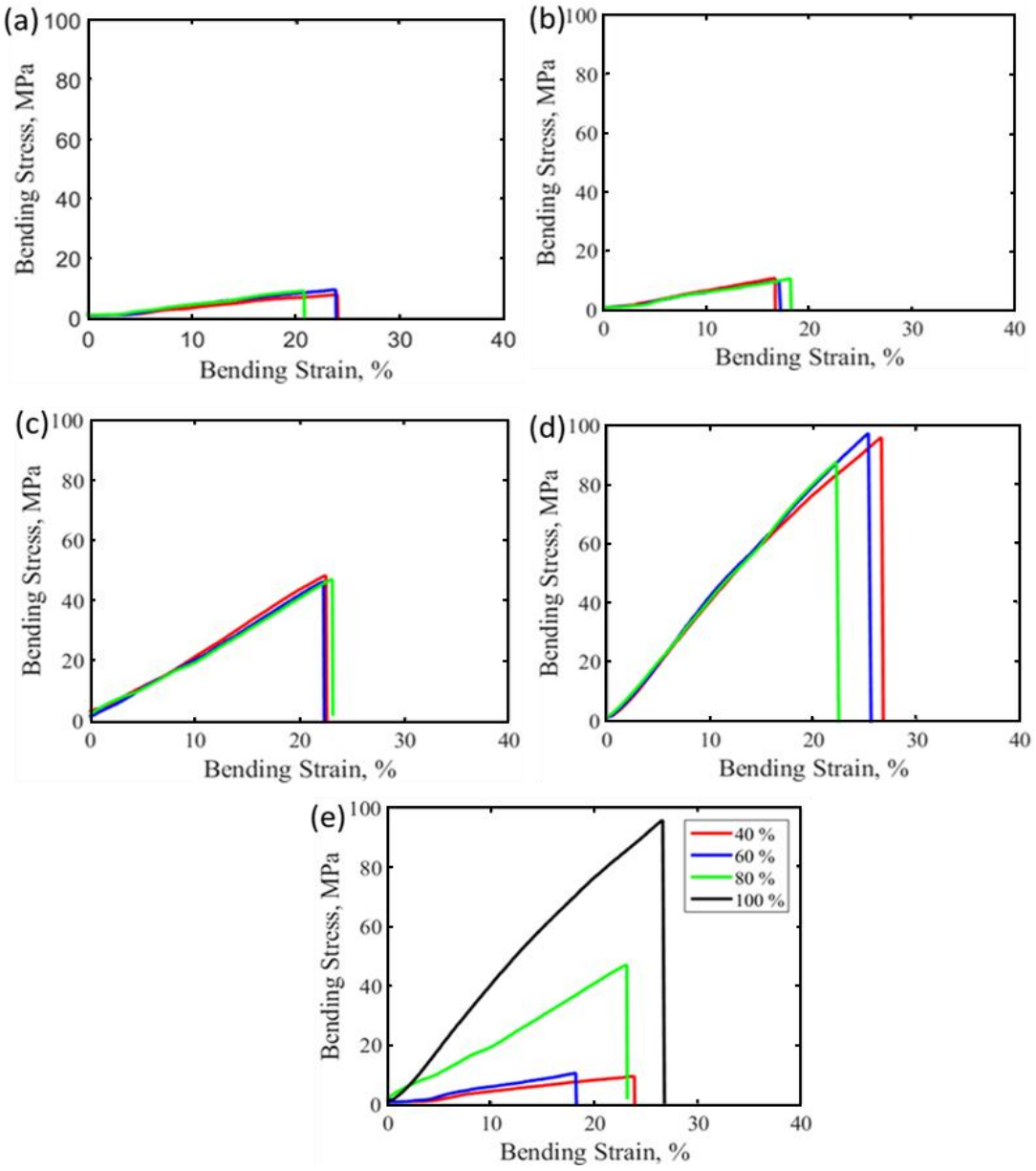

Figure 4. Variation of bending stress-bending strain with the function of infill density of (three replicas: blue, red and green represented the trail-1, trail-2, and trail-3, respectively): (a) 40%; (b) 60%; (c) 80%; (d) 100%; (e) combined graph.

Table 4. Observed 3PBT of FDMed PLA specimen.

Sample		P_force,	P_Disp,	F_Stress,	F_Strain,	Stiffness,	F_modulus,G	F_toug,
40%	Trail_1	399.6	2.08	7.97	24.06	145.70	2.77	416.60
	Trail_2	352.0	2.40	9.60	23.86	165.50	3.59	422.40
	Trail_3	423.0	2.39	9.13	20.84	177.40	2.92	505.50
	Avg	391.53	2.29	8.90	22.93	162.90	3.09	448.23
	SD	36.18	0.18	0.84	1.81	16.00	0.43	49.74
	SE	20.89	0.11	0.48	1.05	9.2	0.25	28.72
60%	Trail_1	471.9	1.82	10.84	16.69	266.60	4.80	429.40
	Trail_2	432.2	1.71	9.78	17.05	207.60	4.32	369.50
	Trail_3	478.9	1.66	10.68	18.23	207.60	4.32	397.50
	Avg	461.00	1.73	10.43	17.32	227.20	4.48	398.80
	SD	25.20	0.08	0.57	0.81	34.10	0.28	29.97
	SE	14.50	0.05	0.33	0.47	19.70	0.16	17.30
80%	Trail_1	2084.00	2.31	48.38	22.60	987.20	17.41	2407.00
	Trail_2	2137.00	2.25	46.23	22.35	938.60	16.88	2404.13
	Trail_3	2040.00	2.23	47.16	23.17	949.20	16.64	2274.60
	Avg	2087.00	2.26	47.26	22.71	958.30	16.98	2361.91
	SD	48.60	0.04	1.08	0.42	25.60	0.39	75.63
	SE	28.00	0.02	0.62	0.24	14.80	0.23	43.66
100%	Trail_1	3873.00	2.22	95.89	26.77	1755.70	28.79	4299.00
	Trail_2	4236.00	2.66	97.42	25.60	1644.30	27.50	5633.88
	Trail_3	4304.00	2.53	78.30	21.11	1634.30	27.50	5444.56
	Avg	4137.70	2.47	90.54	24.49	1678.10	27.93	5123.81
	SD	231.70	0.23	10.62	2.99	67.40	0.75	722.27
	SE	133.80	0.13	6.13	1.73	38.90	0.43	417.00

*Note: P_force: peak force; P_Disp: peak displacement; F_Stress: fracture stress; F_Strain: fracture strain; F_modulus: flexural modulus; F_tough: flexural toughness; SD: standard deviation; SE: standard error, Avg: average.

3.3. Flexural toughness

Flexural toughness was determined from the area under the bending load-displacement curve (ASTM C1018 [24]). Figure 5 shows the bending force-displacement response of PLA specimen with different ID percentage. The response behavior was the same as those in bending stress and bending strain. Increasing the ID percentage was resulted to increase in the stiffness of the PLA specimens. The stiffness of the PLA specimen at each ID percentage was calculated and stated in Table 4. The result shows that the stiffness of the PLA specimen raised significantly as the ID percentage increased due to the increasing contact between the layers consequently increases the bonding strength. In general, the toughness of the PLA specimen increased dramatically at 80% and 100% ID samples. Mainly at 100% ID, the toughness increased more than two times of the 80% ID. Figure 6 illustrates the average toughness of the PLA specimen as a function of the ID percentage.

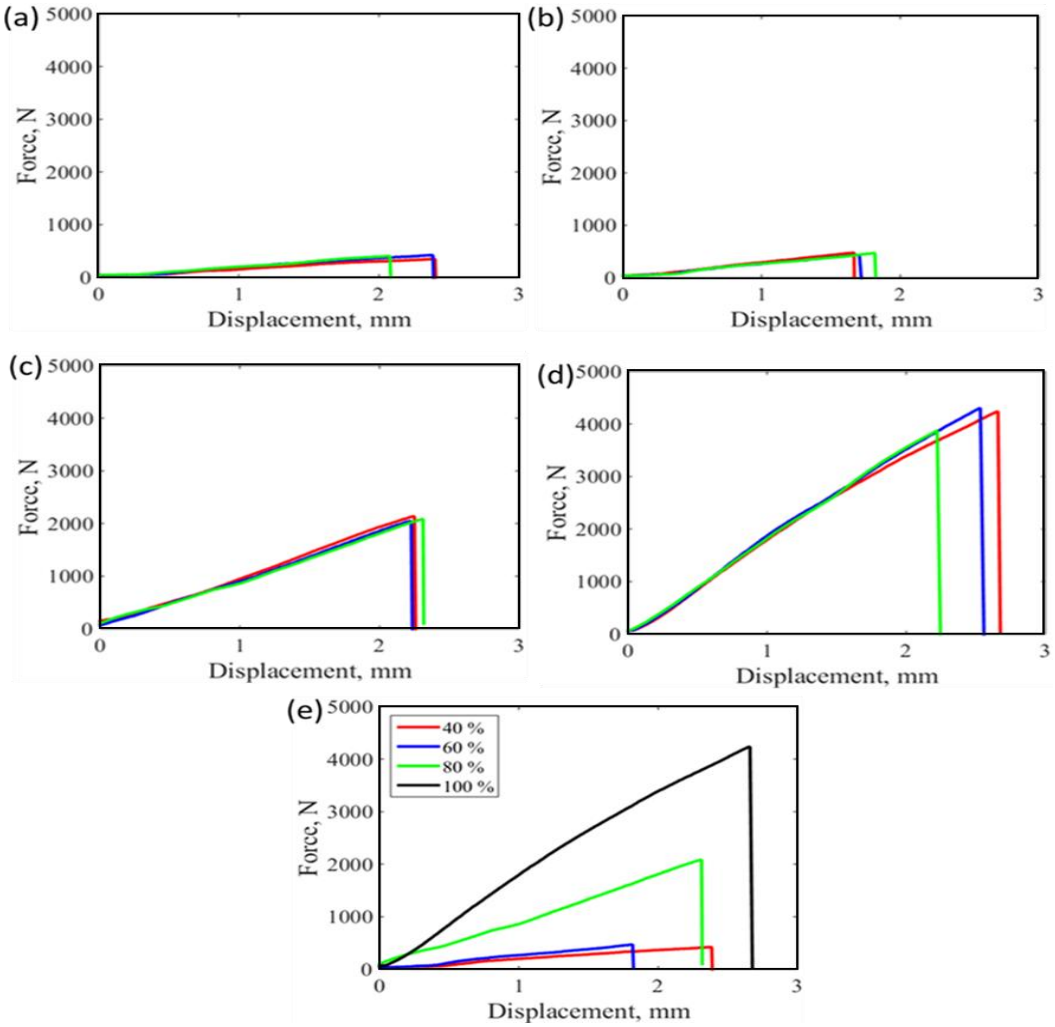

Figure 5. Variation of bending load-displacement with the function of infill density of (three replicas: blue, red and green represented the trail-1, trail-2, and trail-3 respectively): (a) 40%; (b) 60%; (c) 80%; (d) 100%; (e) combined graph.

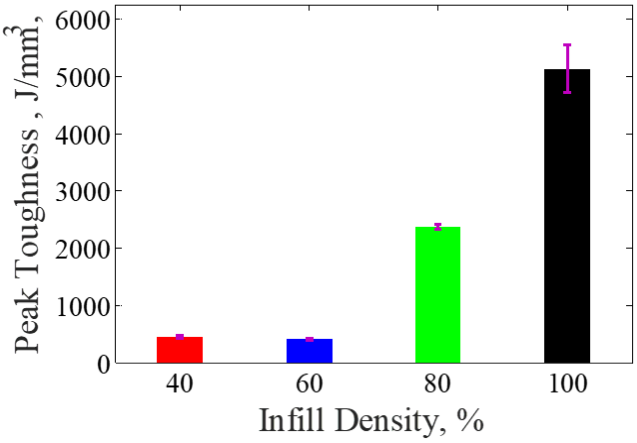

Figure 6. The average toughness of the PLA specimen as a function of the infill density.

3.4. Flexural modulus

Flexural modulus was calculated as per Eq 3 and the same is reported in Table 4. Figure 7 shows the variation of flexural modulus with the function of ID. The average flexural modulus was 46, 67, 254, and 419 GPa for 40%, 60%, 80%, and 100% ID respectively. The results were revealed that flexural modulus was increased slightly to 60% and then increased significantly. The lower value of flexural modulus for 40% and 60% ID samples was due to the presence of more air gap (porosity) which decreased the strength of printed samples. However, 80% ID sample produced a higher value of flexural modulus when compared to 40% and 60% ID samples and lower than 100% ID sample. This result was due to less air gap (less porosity) between layers which increased the strength. 100% ID sample exhibited an extremely high value of flexural modulus due to no air gap was attained (0% porosity) and more bonding strength among layers was achieved. Among the investigated samples, 80% ID sample possess considerable flexural modulus which can be recommended for tissue/bone engineering applications where strength and porous characteristics are important. Overall, the results indicate that the ID percentages have a great effect on the modulus of elasticity of the PLA specimen.

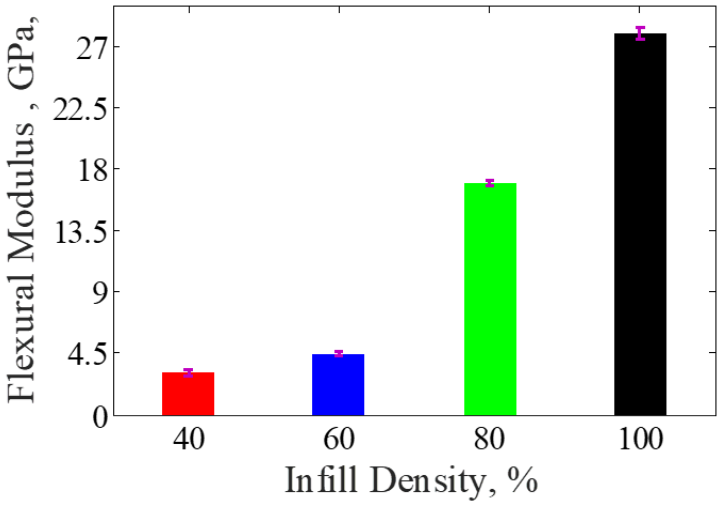

Figure 7. Variation of flexural modulus with the function of infill density.

3.5. Energy absorption capacity

Bone/tissue engineering parts require more energy absorption capacity during its applications [25], so that the bone/tissue parts can dissipate the kinetic energy obtained from uncertainty. It has to be controlled regularly. The energy absorption capacity of 3D printed PLA parts can be determined from the area under the curve of bending stress-bending strain as per Eq 4:

$$U_b = \int_0^{\varepsilon_b} \sigma_b d\varepsilon_b \tag{4}$$

where U_b is the energy absorption capacity in J/m^3, σ_b is the bending stress in N/m^2, and ε_b is the

bending strain in m/m. Table 5 and Figure 8 illustrate the energy absorption capacity as a function of the ID. However, it is needed to calculate the energy absorption capacity in J/kg as per Eq 5:

$$U_{bm} = \frac{U_b}{\rho} \tag{5}$$

where U_{bm} is the energy absorption capacity in J/kg, ρ is the density of the sample in kg/m^3. The density of each infill density was determined using the rule of the mixture as per Eq 6 which is illustrated in Table 5.

$$\rho = f_{pla}\rho_{pla} + f_{air}\rho_{air} \tag{6}$$

where f_{pla} is the volume fraction of PLA material, ρ_{pla} is the density of PLA material (1240 kg/m^3), f_{air} is the volume fraction of air, ρ_{air} is the density of air (1180 kg/m^3 @ 25 ℃). Figure 8 shows the variation of energy absorption capacity of PLA parts with the function of ID in which the energy absorption capacity was considerably high for 80% and 100% ID samples. The energy absorption capacity of 80% ID samples was 4369 J/kg which is matched with expandable polystyrene foam which has 4550 J/kg at 55% density [22]. Therefore, the 80% ID sample can be suggested for bone/tissue engineering applications as it possesses considerable strength and substantial energy absorption capacity.

Table 5. The energy absorption capacity of 3D printed PLA parts.

Infill density, %	Density of sample, kg/m^3	Energy absorption, kJ/m^3	Energy absorption, J/kg
40	1204	1019 ± 64	864 ± 53
60	1216	904 ± 40	743 ± 33
80	1228	5366 ± 100	4369 ± 81
100	1240	11190 ± 1466	9024 ± 1183

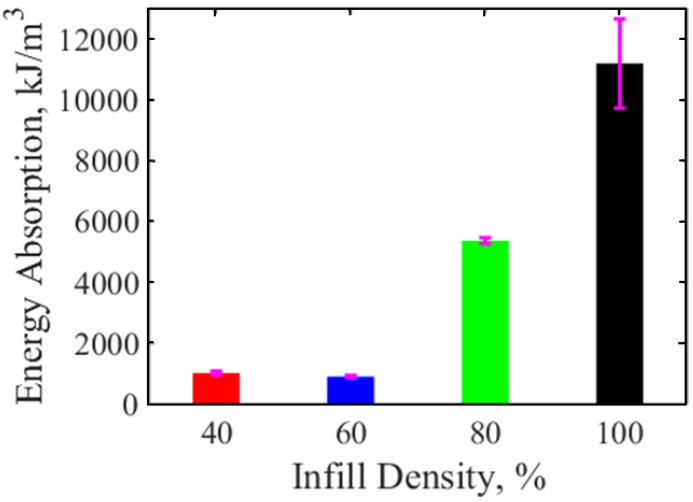

Figure 8. The energy absorption capacity of the PLA specimen with the function of the infill density.

3.6. Fracture surface investigation

Figure 9 shows the fracture surface characteristics of 3D printed parts after 3PBT with the function of ID at different magnification (65×, 200×, and 800×). In general, the fracture surface of the tested samples in the present investigation revealed two main features: the first is the smooth area and the second is the rough region.

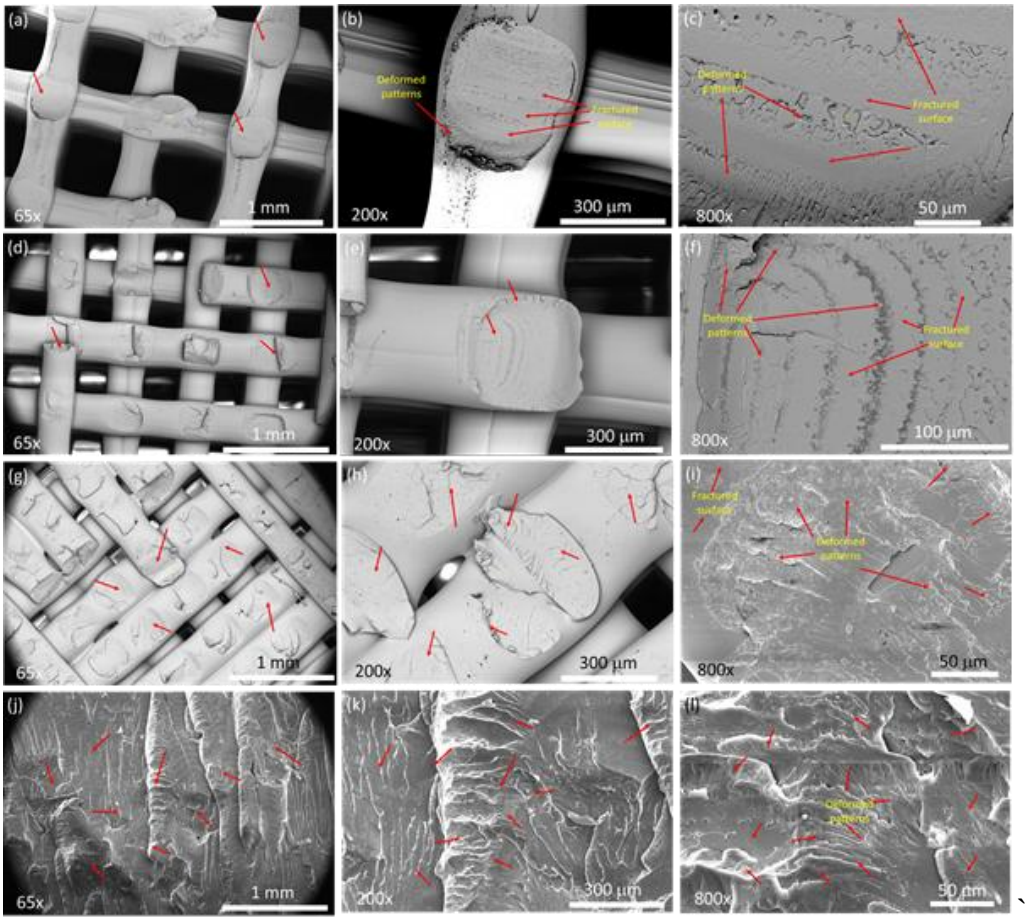

Figure 9. Fracture surface topography of 3D printed PLA parts after 3PBT in different magnifications of (a) 40%-65×; (b) 40%-200×; (c) 40%-800×; (d) 60%-65×; (e) 60%-200×; (f) 60%-800×; (g) 80%-65×; (h) 80%-200×; (i) 80%-800×; (j) 100%-65×; (k) 100%-200×; and (l) 100%-800×.

The smooth area is an indication of the brittle fracture mode while the rough region which includes the deformation patterns is an indication of the ductile rupture. It was observed from Figure 9 that the brittle fracture mechanism is predominant in the sample with 40% ID and the ductile fracture mode is the principle fracture mechanism when increasing the ID to 100%. Increasing the ID from 40% to 100% resulted in increasing the tendency to ductile fracture at the expense of brittle fracture mode. These observations can be attributed to the fact that 40% ID samples contain a large volume fraction of porosity which resulted in low deformability and more brittleness of the samples, as a consequence brittle failure was the main mechanism in this case.

On the other hand, increasing the density of the sample (for example 100% ID sample) resulted in improved ductility and deformability and consequently, ductile failure was the principal mechanism. From Figure 9, at low magnification (65×), it was clear that the 40% ID sample was produced more air gap (porosity) due to fewer layers and more area of smooth fracture surfaces which is an indication to brittle fracture. Due to this, the 40% ID sample was not produced more bending stress, flexural modulus, energy absorption capacity, and stiffness (Figures 4–6, Figure 8, Tables 4 and 5).

However, the observed air gap (porosity) was decreased with the function of ID (see at low magnification, 65×) which indicates the presence of more number of layers consequently increases the strength. Further, increasing of a rough region of deformation patterns and decreasing of the area of smooth fracture surface were observed with the function of ID increases (see at 800 × in Figure 9).

These results were revealed that the ductile characteristic of 3D printed parts was increased with increasing of ID which led to increasing the flexural properties (Figures 4–6, Figure 8, Tables 4 and 5). Besides, from Figure 9, it was ensured that there were no open-up crazes, crater, and voids appeared over the fracture surfaces (Figure 9) which indicate good quality of printed parts obtained from the FDM printer irrespective of ID. In the present study, PLA specimens with different ID were printed in the FDM 3D printer and then the flexural behavior was investigated using 3PBT as per the ASTM standard. Based on the investigated results of surface topography shown in Figure 3; flexural behavior displayed in Figure 4 through Figure 7 and Table 4; energy absorption capacity illustrated in Figure 8 and Table 5; and fracture surface analysis presented in Figure 9; 80% ID and 100% ID PLA samples exhibited improved properties which can be recommended for bio-degradable and bio-implant applications. 3D printed PLA materials can be used to manufacture implant parts such as a screw, rod, mesh and pins for the human tissue parts which never harm the organs.

4. Conclusion

This research work has studied the effect of varying the ID percentage (porous) of the 3D printed of PLA specimens using 3PBT. The cylindrical PLA printed specimens were subjected to 3PBT using hemispherical pin loading. The characteristics of the 3PBT in terms of the peak force, peak displacement, fracture stress, fracture strain, stiffness, flexural modulus, and flexural toughness were determined. The experimental results appear that the 3PBT characteristics (Tables 4 and 5) improved as the ID percentage increased. Specifically, the characteristics of the 3PBT behavior have improved dramatically at 80% and 100% ID. Besides, the results show that the energy absorption capacity of the 3D printed PLA specimen improved dramatically as the ID increased. The possible explanation for this was due to that reducing the porosity result in increasing the contact and bonding between the layers which made the PLA specimen to absorb higher energy. From the microstructural examination, the brittle fracture features (smooth region) and ductile fracture characteristics (deformed patterns) were observed in all ID percentages. Qualitatively, the ductile fracture mode features (deformed pattern) increased as the ID percentage increased.

Acknowledgements

The authors acknowledge to the Digital Manufacturing Laboratory, Mechanical Engineering Department, Qassim Engineering College, Qassim University, Saudi Arabia for the financial support and research facilities used to carry out this research work.

Conflicts of interests

The authors declare no conflict of interest.

References

1. Francis V, Jain PK (2018) Investigation on the effect of surface modification of 3D printed parts by nanoclay and dimethyl ketone. *Mater Manuf Process* 33: 1080–1092.
2. Ahn S-H, Montero M, Odell D, et al. (2002) Anisotropic material properties of fused deposition modeling ABS. *Rapid Prototyp J* 8: 248–257.
3. Lanzotti A, Grasso M, Staiano G, et al. (2015) The impact of process parameters on mechanical properties of parts fabricated in PLA with an open-source 3-D printer. *Rapid Prototyp J* 21: 604–617.
4. Onwubolu GC, Rayegani F (2014) Characterization and optimization of mechanical properties of ABS parts manufactured by the fused deposition modelling process. *Int J Manuf Eng* 2014: 598531.
5. Domingo-Espin M, Puigoriol-Forcada JM, Garcia-Granada AA, et al. (2015) Mechanical property characterization and simulation of fused deposition modeling polycarbonate parts. *Mater Des* 83: 670–677.
6. Popescu D, Zapciu A, Amza C, et al. (2018) FDM process parameters influence over the mechanical properties of polymer specimens: A review. *Polym Test* 69: 157–166.
7. Rankouhi B, Javadpour S, Delfanian F, et al. (2016) Failure analysis and mechanical characterization of 3D printed ABS with respect to layer thickness and orientation. *J Fail Anal Prev* 16: 467–481.
8. Li H, Wang T, Sun J, et al. (2018) The effect of process parameters in fused deposition modelling on bonding degree and mechanical properties. *Rapid Prototyp J* 24: 80–92.
9. Liu X, Zhang M, Li S, et al. (2017) Mechanical property parametric appraisal of fused deposition modeling parts based on the gray Taguchi method. *Int J Adv Manuf Technol* 89: 2387–2397.
10. Mohamed OA, Masood SH, Bhowmik JL (2015) Optimization of fused deposition modeling process parameters: a review of current research and future prospects. *Adv Manuf* 3: 42–53.
11. Sood AK, Ohdar RK, Mahapatra SS (2010) Parametric appraisal of mechanical property of fused deposition modelling processed parts. *Mater Des* 31: 287–295.
12. Chacón JM, Caminero MA, García-Plaza E, et al. (2017) Additive manufacturing of PLA structures using fused deposition modelling: Effect of process parameters on mechanical properties and their optimal selection. *Mater Des* 124: 143–157.
13. Tymrak BM, Kreiger M, Pearce JM (2014) Mechanical properties of components fabricated with open-source 3-D printers under realistic environmental conditions. *Mater Des* 58: 242–246.

14. Fernandez-vicente M, Calle W, Ferrándiz S, et al. (2016) Effect of infill parameters on tensile mechanical behavior in desktop 3D printing. *3D Print Addit Manuf* 3: 183–192.
15. Ziemian C, Sharma M, Ziemian S (2012) Anisotropic mechanical properties of ABS parts fabricated by fused deposition modelling, In: Gokcek M, *Mechanical Engineering*, Rijeka: TechOpen, 158–150.
16. Tsouknidas A, Pantazopoulos M, Katsoulis I, et al. (2016) Impact absorption capacity of 3D-printed components fabricated by fused deposition modelling. *Mater Des* 102: 41–44.
17. Torres J, Cotelo J, Karl J, et al. (2015) Mechanical property optimization of FDM PLA in shear with multiple objectives. *Jom* 67: 1183–1193.
18. Ruhatiya C, Singh S, Goyal A, et al. (2020) Electrochemical performance enhancement of sodium-ion batteries fabricated with $NaNi_{1/3}Mn_{1/3}Co_{1/3}O_2$ cathodes using support vector regression-simplex algorithm approach. *J Electrochem Energy Convers Storage*. Available from: https://doi.org/10.1115/1.4044358.
19. Camargo JC, Machado ÁR, Almeida EC, et al. (2019) Mechanical properties of PLA-graphene filament for FDM 3D printing. *Int J Adv Manuf Technol* 103: 2423–2443.
20. Aw Y, Yeoh C, Idris M, et al. (2018) Effect of printing parameters on tensile, dynamic mechanical, and thermoelectric properties of FDM 3D printed CABS/ZnO composites. *Materials* 11: 466.
21. ASTM C (1997) Standard test method for flexural toughness and first-crack strength of fiber-reinforced concrete (using beam with third-point loading). C-1018.
22. Di Landro L, Sala G, Olivieri D (2002) Deformation mechanisms and energy absorption of polystyrene foams for protective helmets. *Polym Test* 21: 217–228.
23. Ramnath BV, Jeykrishnan J, Elanchezhian C, et al. (2017) Investigation of flexural behaviour of polymer composite golf shaft. *Mater Today Proc* 4: 9341–9345.
24. Grasso M, Azzouz L, Ruiz-Hincapie P, et al. (2018) Effect of temperature on the mechanical properties of 3D-printed PLA tensile specimens. *Rapid Prototyp J* 24: 1337–1346.
25. Alaboodi AS, Sivasankaran S (2018) Experimental design and investigation on the mechanical behavior of novel 3D printed biocompatibility polycarbonate scaffolds for medical applications. *J Manuf Process* 35: 479–491.

AIMS Press